Optimal Modeling and County-Level Applications for the Spatial Prediction of Soil Organic Matter: A Case Study of Thirteen Counties in the Yellow River Basin

Ziyang Zhang[a], Mengmeng Wu[a],ZiYi Hu[a], Haibin Wang[a,b*],LiWen Liu[a,b*],Yaodong Jing[a,b],Mingxing Qin[a,b],Ke Hu[a,b],Qi Liu[c]

[a] College of Resource and Environment, Shanxi Agricultural University, Taigu, 030801, Shanxi, China
[b]Soil Health Laboratory in Shanxi Province, Taiyuan, 030031, Shanxi, China

[c] Shanxi Province Geological Environment Monitoring and Ecological Restoration Center, Taiyuan, 030000, Shanxi, China

*Corresponding author at present.

E-mail: whb4052@163.com(Haibin Wang), Liuliwen545@163.com(Liwen Liu)

Abstract. Soil organic matter (SOM) is a key indicator for assessing soil health and the carbon sequestration potential, and its precise spatial prediction is vital for ensuring sustainable agricultural development. Machine learning has emerged as a core tool in digital soil mapping. However, in complex landscapes such as the Yellow River Basin, the selection of models and the translation of their predictions into county-level governance remain uncertain. To address these issues, this study focused on thirteen counties in the Yellow River Basin. We systematically established five machine learning models, namely, random forest (RF), ridge regression, LASSO regression, gradient boosting, and support vector regression models, and obtained 172 soil samples and multiple environmental variables to predict SOM. We optimized the models through recursive feature elimination and cross-validation and comprehensively evaluated their performance on the basis of metrics such as the coefficient of determination (R^2) and root mean square error (RMSE). The results indicated that the random forest model achieved the best prediction accuracy and stability (test set $R^2 = 0.56$; RMSE = 3.36 g/kg). Spatial distribution maps generated from this model revealed a distinct SOM pattern across the study area encompassing high values in the east and west and low values in the central region. County-level comparative analysis revealed that compared with counties dominated by intensive agriculture (e.g., Hejin), counties with high forest cover (e.g., Jixian) exhibited significantly higher average SOM contents. This study confirms that the random forest model is a high-precision prediction model suitable for this region. The findings not only reveal key environmental drivers but also, more importantly, provide a county-level comparable SOM spatial dataset and demonstrate clear intercounty differences, directly supporting the formulation of differentiated soil conservation policies. For instance, the results of this study offer a systematic basis for delineating SOM enhancement and conservation zones and for implementing corresponding management measures with precision.

Keywords. Soil organic matter; Machine learning; Random forest; Spatial prediction; Yellow River Basin; County scale; Precision agriculture

1 Introduction

Soil organic matter (SOM), as a core component of soil quality, notably influences soil fertility, crop productivity, and the global carbon cycle [1, 2]. Accurately determining its spatial distribution is a prerequisite for implementing conservation tillage, assessing the soil carbon sequestration potential, and formulating sustainable land management strategies [3]. With the development of geographic information technologies and data science, digital soil mapping, through the integration of point-based soil observations with continuous environmental covariates, has become the mainstream approach for generating high-resolution soil property maps [4]. In this process, machine learning algorithms, owing to their notable nonlinear modeling capabilities, have been widely applied to the spatial prediction of SOM and have demonstrated substantial potential.

Although various machine learning models (e.g., random forest, support vector machines, and gradient boosting models) are theoretically applicable to this task, their prediction performance highly depends on specific data characteristics and geographic contexts [5]. In the Yellow River Basin, which constitutes a typical eco–agricultural region characterized by diverse landforms and intertwined land use patterns, systematic comparisons and evaluations remain lacking to determine which model can achieve the optimal accuracy and robustness for the spatial prediction of soil organic matter. More importantly, existing studies often stop at comparing model accuracy levels and producing spatial maps without further translating the results of model selection and the generated spatial information into differentiated management guidance directly applicable at the county level. This gap has led to a last-mile disconnect between scientific research and local governance practices.

Therefore, the long-term objective of this study is to provide a comprehensive framework (from methodological optimization to spatial decision support) for refined soil resource management and green agricultural development in the Yellow River Basin. To achieve this goal, we set the following three progressively specific objectives: (1) to systematically compare the performance levels of five models, i.e., random forest, ridge regression, LASSO regression, gradient boosting, and support vector regression models, in predicting soil organic matter across thirteen counties in the Yellow River Basin and to identify the optimal prediction model; (2) to generate high-confidence spatial distribution maps of soil organic matter and to quantitatively analyze the differences in SOM contents among the thirteen county-level administrative units; and (3) to integrate spatial patterns with county-level statistical results to explore their specific applications and value in guiding differentiated soil conservation and precision fertilization practices.

2 Materials and Methods

2.1 Overview of the Study Area

The study area is located along the Jin–Shaanxi Gorge in the middle reaches of the Yellow River, encompassing thirteen counties (or cities) in Shanxi Province from north to south. The region is characterized by complex terrain and a temperate continental monsoon climate, with land use dominated by dryland agriculture and ecological forests. In this study, we collected a total of 172 surface soil (0–20 cm) samples for organic matter measurement. The environmental covariates included

topographic attributes derived from a digital elevation model, vegetation indices calculated from Landsat imagery, and spatial data on climate and land use. We processed all the data uniformly to a spatial resolution of 30 m.

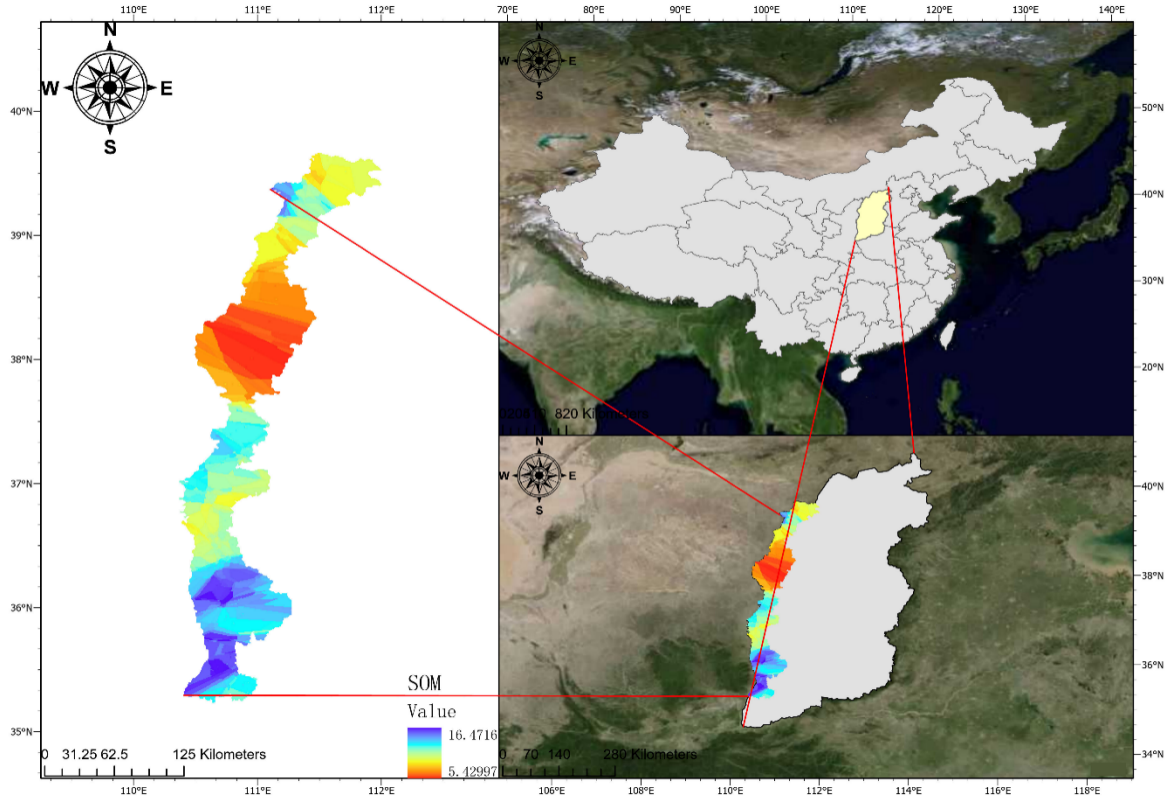

Figure 1: Spatial Distribution of Thirteen Counties (or Cities) in the Study Area

2.2 Data Sources and Preprocessing

Soil Data: In the autumn of 2023, we collected a total of 172 surface soil samples (0–20 cm) via a stratified random sampling method. The soil organic matter (SOM) content was determined through the potassium dichromate external heating method. Basic statistical characteristics of the samples revealed that the SOM contents ranged from 5.14 to 55.20 g/kg, with a mean value of 20.15 g/kg and a coefficient of variation of 30.06%, indicating that the degree of variability did not preclude spatial predictive modeling.

Environmental Covariates: We collected a total of 33 environmental variables, grouping them into four categories, namely, (a) topographic indices derived from the 30-m ASTER GDEM product, such as slope and topographic wetness index; (b) vegetation indices calculated from Landsat 8 imagery, including NDVI and EVI; (c) climatic factors, including the mean annual temperature and mean annual precipitation; and (d) soil type and land use data. We resampled all the datasets to a uniform 30-m resolution and conducted spatial registration.

2.3 Machine Learning Modeling and Optimization

In this study, five models were selected for comparison, namely, random forest, gradient boosting, support vector regression, ridge regression, and LASSO regression models. To increase efficiency, we compared two hyperparameter optimization strategies, i.e., grid search and random search. The results indicated that a random search required only 5.4% of the time needed for the grid search (17.2 s vs. 317.7 s) while achieving comparable accuracy. Therefore, we ultimately adopted a random search for hyperparameter tuning.

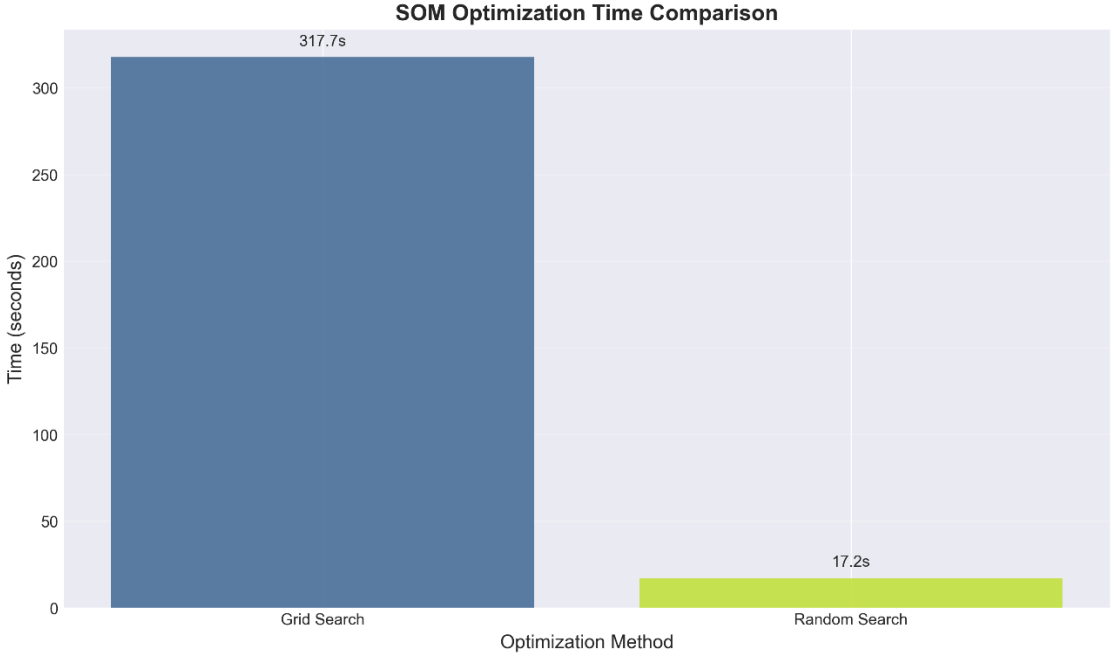

Figure 2: Comparison of the Time Costs for Hyperparameter Optimization

Before model construction, we employed recursive feature elimination for feature selection to remove redundancy. We randomly assigned 70% of the total samples to the training set for model training and adopted 5-fold cross-validation for hyperparameter tuning, while the remaining 30% served as an independent test set for final model performance evaluation. The primary evaluation metrics included the coefficient of determination (R^2), root mean square error (RMSE), and mean absolute error (MAE).

Random Forest: This model is an ensemble bagging algorithm based on decision trees that is well suited for resolving high-dimensional data and complex relationships.

Ridge Regression and LASSO Regression: Both are linear models that prevent overfitting by incorporating L2 and L1 regularization, respectively, with the LASSO regression model additionally providing feature selection capability.

Gradient Boosting: This model constitutes a boosting algorithm that iteratively trains weak learners to reduce residual errors.

Support Vector Regression: This algorithm relies on kernel functions to map data into high-dimensional space to achieve nonlinear fitting.

We implemented all the models using the scikit-learn library in Python. To eliminate redundant information and increase model efficiency, we applied recursive feature elimination before training to select feature subsets for each model. We optimized the model hyperparameters via a grid search combined with 5-fold cross-validation.

2.4 Model Evaluation and Spatial Analysis

We randomly divided the dataset into training and independent test sets at a ratio of 70/30. We used the coefficient of determination (R^2) and the root mean square error (RMSE) as the primary metrics to evaluate model performance. We assessed model robustness on the basis of the 10-fold cross-validation results. We then applied the best-performing model to the entire study area for spatial prediction, thereby generating a soil organic matter distribution map. On the basis of this map, we extracted the mean SOM content within the administrative boundaries of each of the thirteen counties and performed a statistical analysis, employing analysis of variance (ANOVA), to verify the significance of intercounty differences.

2.5 Analysis of Multicollinearity and Feature Selection of Environmental Covariates

Before the prediction models were established, we systematically examined all the continuous environmental covariates to prevent potential negative effects of multicollinearity on model stability, interpretability, and generalizability. We used a Pearson correlation matrix heatmap (Figure 3) to visually illustrate the degree of linear correlation among the variables.

The analysis indicated that certain environmental variables were strongly correlated ($|r| > 0.7$). For instance, we observed strong collinearity between the soil bulk density and soil pH, as well as among several climatic factors, such as the mean annual temperature and growing season temperature. Such high correlations suggest that directly including all the variables in the model, particularly in linear models such as the ridge and LASSO regression models, may distort coefficient estimates, reduce interpretability, and potentially cause overfitting, thereby compromising the predictive reliability of new data.

To ensure the robustness and scientific validity of the models, we employed recursive feature elimination (RFE) for feature selection. This method aims to recursively remove redundant or highly collinear features on the basis of model performance, enabling each machine learning model to process an independent, efficient, and low-redundancy optimal feature subset. This step is crucial for enhancing model generalizability, accelerating the training process, and improving the interpretability of results.

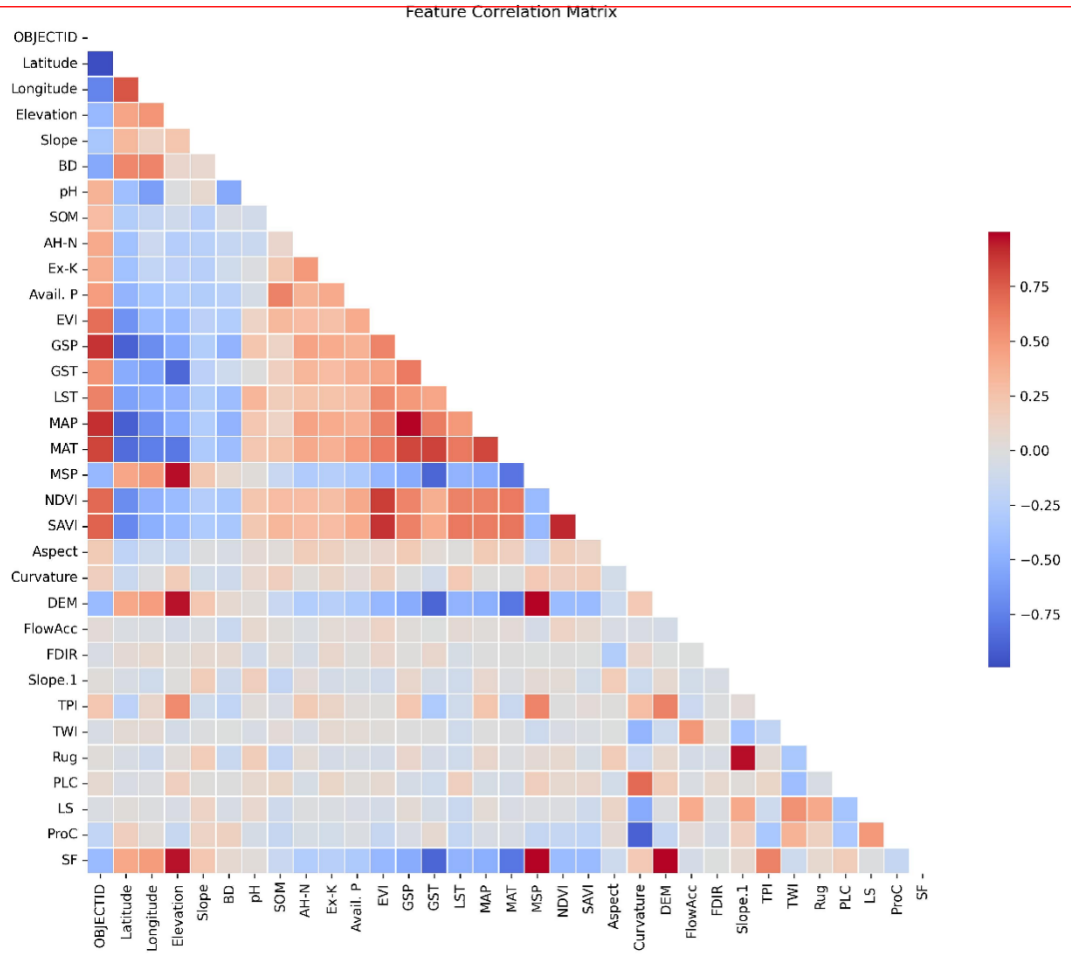

Figure 3: Heatmap of the Pearson Correlation Matrix for the Environmental Covariates

3 Results

3.1 Model Selection

3.1.1 Comprehensive Comparison of Prediction Performance across Multiple Models

To comprehensively evaluate the performance of the five machine learning models in predicting soil organic matter (SOM), in this study, the final accuracy of each model for the independent test set (Table 1) was integrated with their behavioral characteristics in the learning process (Figure 4), thereby providing a holistic analytical perspective that spans from static results to dynamic fitting processes.

Table 1: Prediction Performance of the Five Machine Learning Models for the Independent Test Set

Model	Training Time (sec)	Test R2	Test RMSE
Random Forest	0.254778	0.560467	3.367109
Support Vector Regression	0.002059	0.440146	3.800131
Gradient Boosting	0.2121	0.42299	3.857916
LASSO Regression	0.002994	0.374729	4.016015
Ridge Regression	0.007004	0.366364	4.042791

As indicated in Table 1, the random forest (RF) model achieved the best overall prediction performance for the independent test set, with an R^2 value of 0.560467 and an RMSE of 3.367109 g/kg. The support vector regression (SVR) and gradient boosting (GB) models performed moderately, whereas the two linear models (ridge and LASSO regression models) exhibited a lower prediction accuracy.

However, the final performance for the independent test set provided only a partial assessment. By analyzing the learning curves of each model (Figure 4), we gained more in-depth insights into their generalizability and overfitting risks, which are critical for assessing the reliability of models in practical applications.

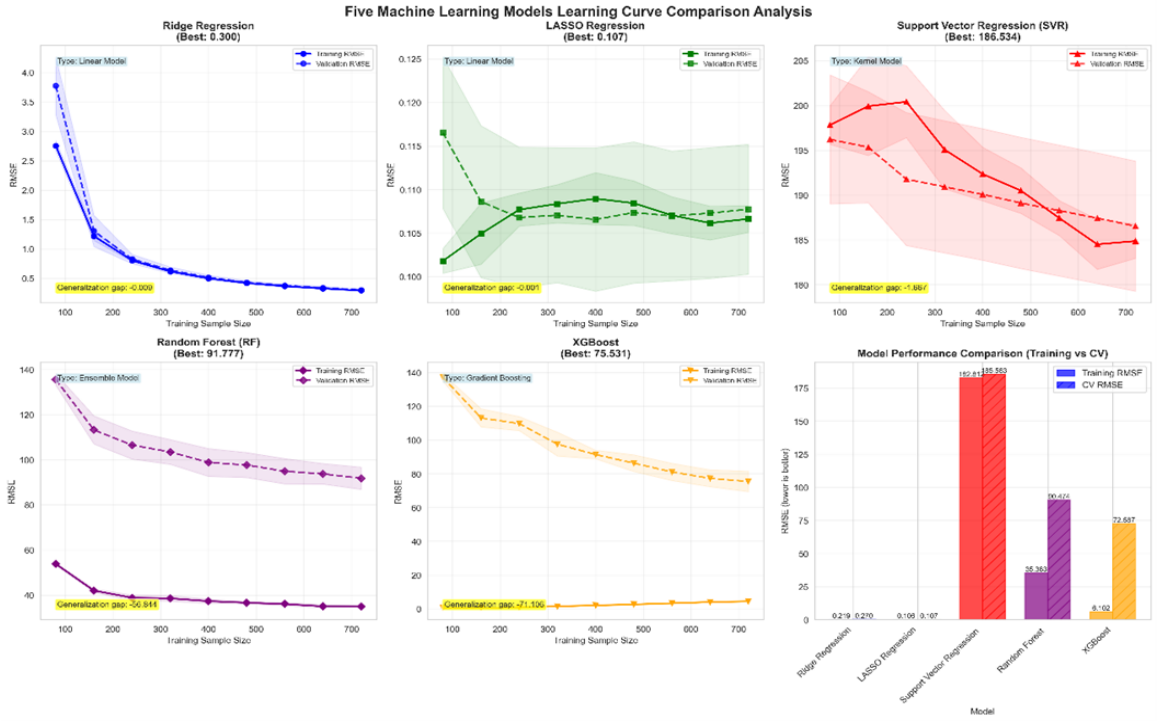

Figure 4: Comparative Analysis of the Learning Curves for the Five Machine Learning Models

An analysis of the learning curves (Figure 4) revealed the inherent differences among the various model families:

The linear models (ridge and LASSO regression models) exhibited excellent stability and generalizability. Their RMSE curves for the training and validation sets almost completely overlapped and rapidly decreased to a stable low level (e.g., the best validation RMSE for the ridge regression model was 0.300), indicating a minimal generalization gap. These findings suggest that these linear models can quickly and efficiently learn stable patterns from limited data with a low risk of overfitting, although their expressive power and the upper limit of the prediction accuracy may be constrained.

In contrast, the ensemble models (random forest and gradient boosting) exhibited typical characteristics of high variance with high bias-correction capability. Their training RMSEs could be reduced to very low levels, but a notable gap occurred between the training and validation RMSE curves, representing a substantial generalizability gap (e.g., the generalizability gap for the random forest model was 0.305). These findings indicate that these models exhibit notable data-fitting capabilities, enabling them to capture complex patterns to increase accuracy, but they also carry a risk of overfitting to the training data, which could lead to performance fluctuations on unseen data.

The support vector regression model (SVR) exhibited intermediate characteristics, with a relatively small generalizability gap (0.107), demonstrating satisfactory generalizability and a certain degree of robustness.

Multimetric comparisons (Figure 5) indicated that the RF model achieved the highest prediction accuracy for the test set, with the highest R^2 value (0.560) and the smallest root mean square error and mean absolute error values (RMSE = 3.367 g/kg; MAE = 2.717 g/kg). However, the difference in R^2 between the training and test sets reached 0.575, indicating that the highest degree of overfitting occurred. Although the gradient boosting model nearly perfectly fit the training set (R^2 = 0.998), its performance on the test set was poor, and it exhibited the highest overfitting metric, suggesting limited generalizability. The linear models (ridge and LASSO regression models) yielded the least overfitting but also relatively low prediction accuracy. In terms of computational efficiency, the training time for all the models was less than 0.3 seconds, satisfying practical application requirements, with the random forest model requiring a moderate duration of 0.25 seconds.

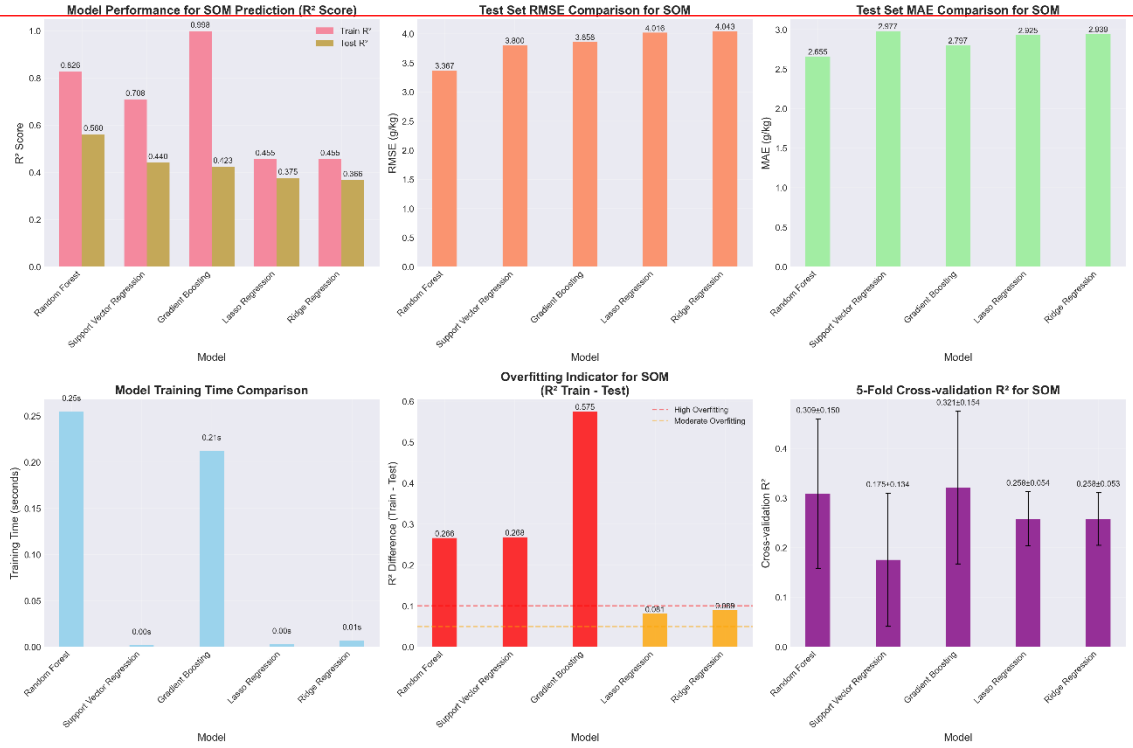

Figure 5: Hexagonal Grid Overview of Model Performance

The model performance heatmap (Figure 6) provides a visual summary of key metrics. The random forest model performed best in terms of the test R^2 (0.560) and test RMSE values (3.367), but its training R^2 value (0.826) was considerably greater than the test value, reaffirming its high-variance nature. The extreme contrast between the training R^2 (0.998) and test R^2 (0.423) values of the GB model was particularly striking in the heatmap. To assess model robustness, the 5-fold cross-validation results (Figure 7) indicated that the random forest method achieved the highest average cross-validation R^2 value (0.309 ± 0.150), with performance fluctuations (standard deviation) that remained within an acceptable range. These findings indicated that despite the risk of overfitting, its prediction performance remained relatively stable across the different data subsets. The support vector regression model and the two linear models exhibited similar and stable cross-validation performance levels, but their average accuracy was relatively low.

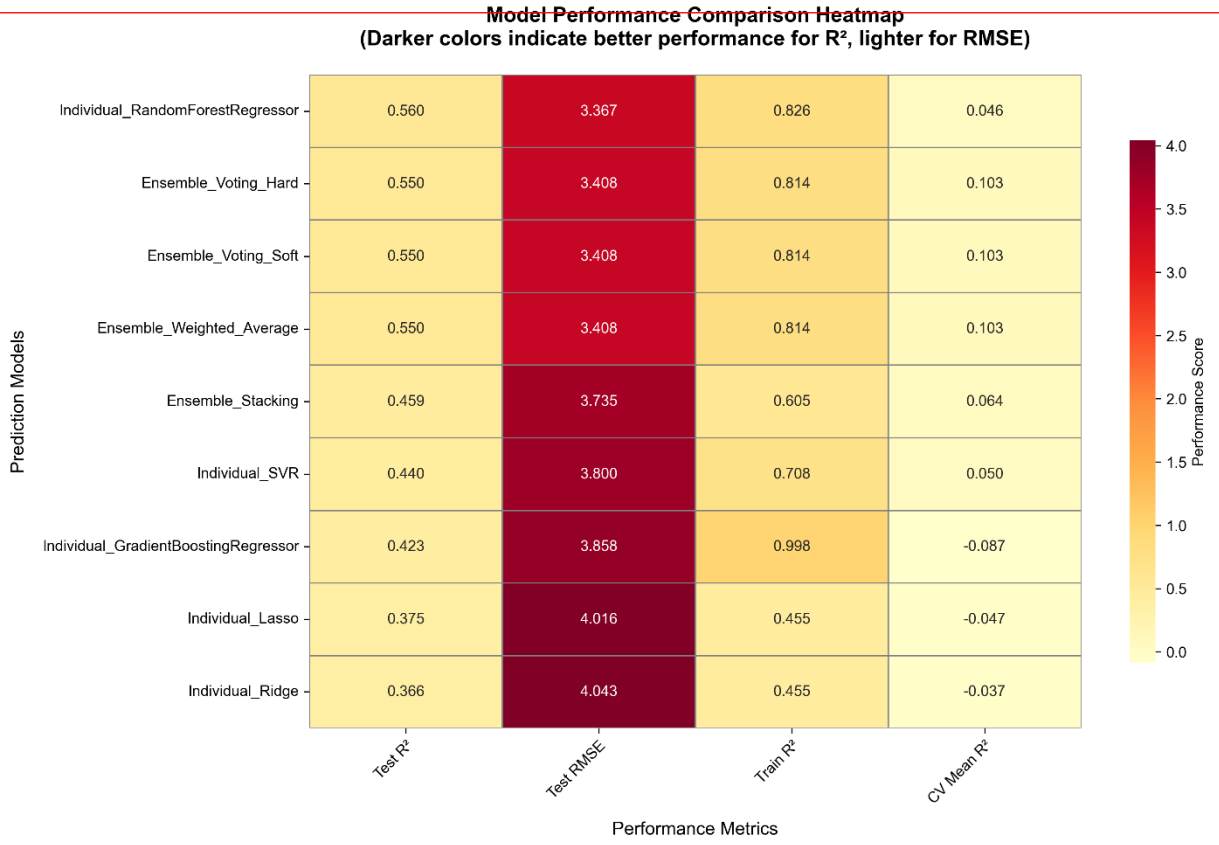

Figure 6: Heatmap Comparison of Model Performance

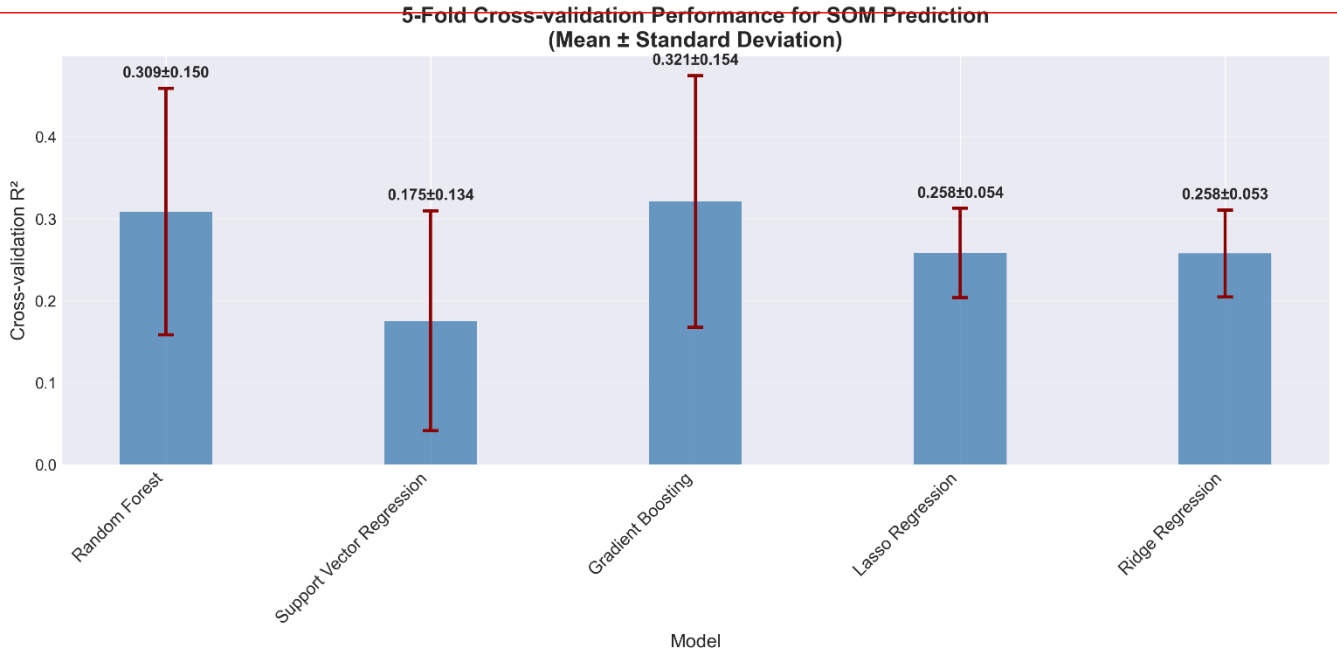

Figure 7: Bar Chart of 5-Fold Cross-Validation Performance

On the basis of the above analyses, the random forest model demonstrated the highest prediction accuracy for the independent test set, and its cross-validation performance was also the most reliable. Therefore, we selected the RF model as the optimal model for subsequent spatial prediction and analysis. However, the clear signs of overfitting indicated that caution is warranted when this model is applied to areas beyond the sampled distribution, and we suggest that ensemble strategies should be considered to enhance robustness.

More cautious and comprehensive conclusions can be drawn from the analysis results presented in Table 1 and Figure 4. In terms of accuracy, under the data conditions of this study, the random forest (RF) model achieved the highest prediction accuracy for the test set and was the optimal choice for performing the current spatial mapping task.

In terms of robustness, the random forest model overfitted the data in the learning process, as indicated by a substantial generalizability gap. This result suggests that its superior accuracy might greatly depend on the representativeness of the current training data. When applied to new areas with sparse sampling or differing environmental conditions, its performance might decline, necessitating careful evaluation. In contrast, although the linear models demonstrated lower absolute accuracy, their minimal generalizability gap indicated excellent robustness and reliability.

Therefore, a trade-off between accuracy and robustness is necessary when models are selected. For scientific research prioritizing the highest accuracy, as in this study, the random forest model is appropriate, but its predictions must be accompanied by uncertainty assessments. For applications emphasizing reliability and interpretability or where the data quality is limited, linear models such as the ridge regression model could serve as a more robust baseline choice.

3.1.2 Visual Analysis of Model Performance: Prediction Accuracy and Residual Analysis

To go beyond single performance metrics (R^2 and RMSE) and to evaluate model prediction behavior from both macrofitting and microerror perspectives, this section provides a systematic visual analysis of the five models.

In the graph of the RF model (Figure 8), the scatter points were clustered most tightly around the ideal prediction line, with the green regression line exhibiting a slope closest to 1. This finding is consistent with its highest test set R^2 value (0.5605) reported in Table 1, visually demonstrating its superior overall prediction accuracy and minimal systematic bias. In contrast, the scatter points for the ridge and LASSO regression models (Figure 8) were more notably dispersed, and the slope of the green regression line was significantly lower than 1, indicating general underestimation of the predicted values. These results conformed with their lower R^2 values (0.3664 and 0.3747, respectively), highlighting the limitations of linear models in capturing the complex soil–environment relationships in this study. The gradient boosting and support vector regression models exhibited an intermediate performance, with accuracy and goodness-of-fit values superior to those of the linear models but slightly inferior to those of the random forest model.

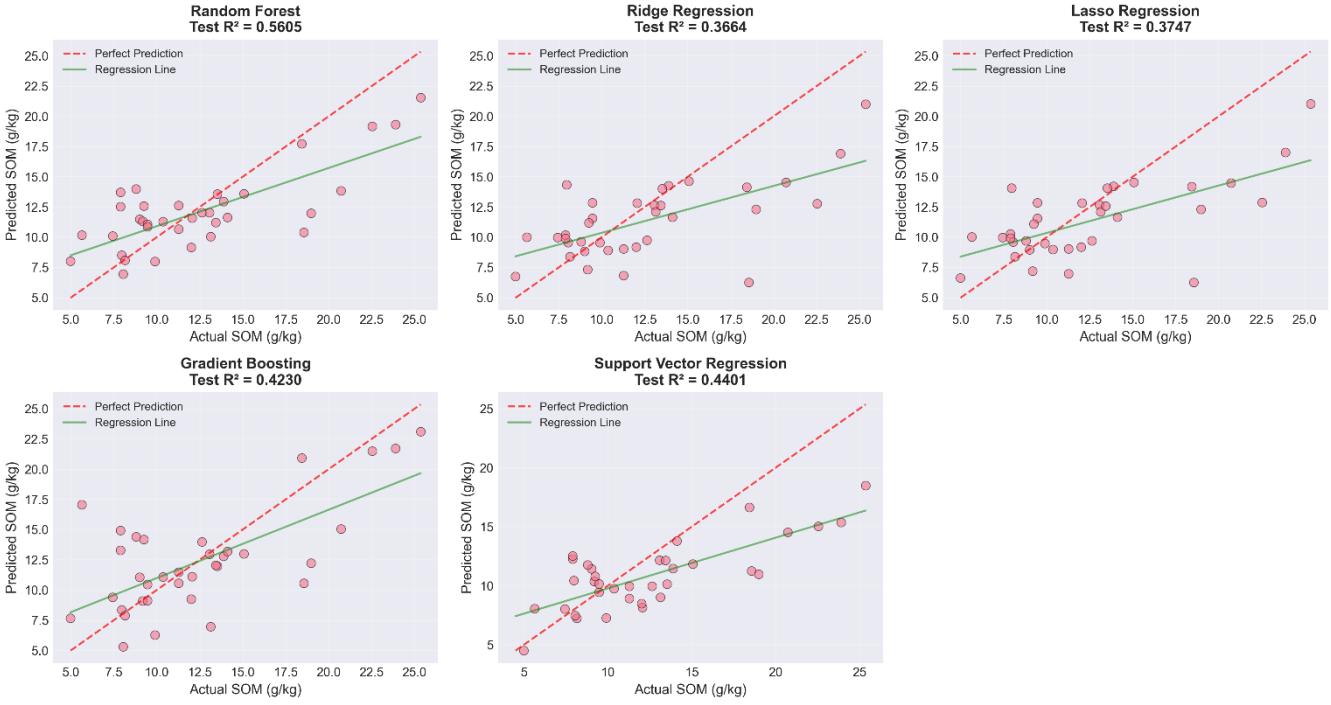

Figure 8: Comparative Scatter Plots of Soil Organic Matter Predictions from the Five Machine Learning Models

To determine the statistical characteristics of the model prediction errors, we generated residual analysis plots for each model. The left column shows scatter plots of residuals versus predicted values, which are used to examine error

homoscedasticity, and the right column shows residual distribution histograms, which are used to assess systematic bias and distribution shape.

The random forest model (Figure 9) exhibited the most favorable residual characteristics, namely, the residuals were evenly and randomly distributed around zero without any apparent trend, indicating that the variance in the prediction errors remained essentially constant across different predicted value levels (satisfying the homoscedasticity assumption). Moreover, the distribution of residuals was approximately symmetric, with a mean (-0.38) closest to zero, confirming that its predictions indicated almost no overall tendency toward over- or underestimation.

The residual plots for the ridge regression, LASSO regression, and support vector regression (Figure 9) revealed common shortcomings, namely, the degree of residual scattering was higher at low predicted values (indicating potential heteroscedasticity), and the means of the residual distribution histograms were significantly positive (ranging from 1.16 to 1.65), consistently indicating systematic underestimation of SOM, which conformed with the observations from the scatter plots (Figure 8).

The residual characteristics of the gradient boosting model were intermediate and inferior to those of the random forest model but superior to those of the other models, with a mean residual (-0.09) close to zero, although its residual distribution exhibited slight skewness.

Combining the macrolevel scatter plots (Figure 8) with the microlevel residual analysis results (Figure 9), the superior performance of the random forest model was verified on the basis of dual visual evidence: it not only achieved the highest prediction accuracy and the best-fit line but also exhibited statistically ideal prediction errors, with minimal systematic bias and stable variance. This made it the most robust and reliable prediction model in this study.

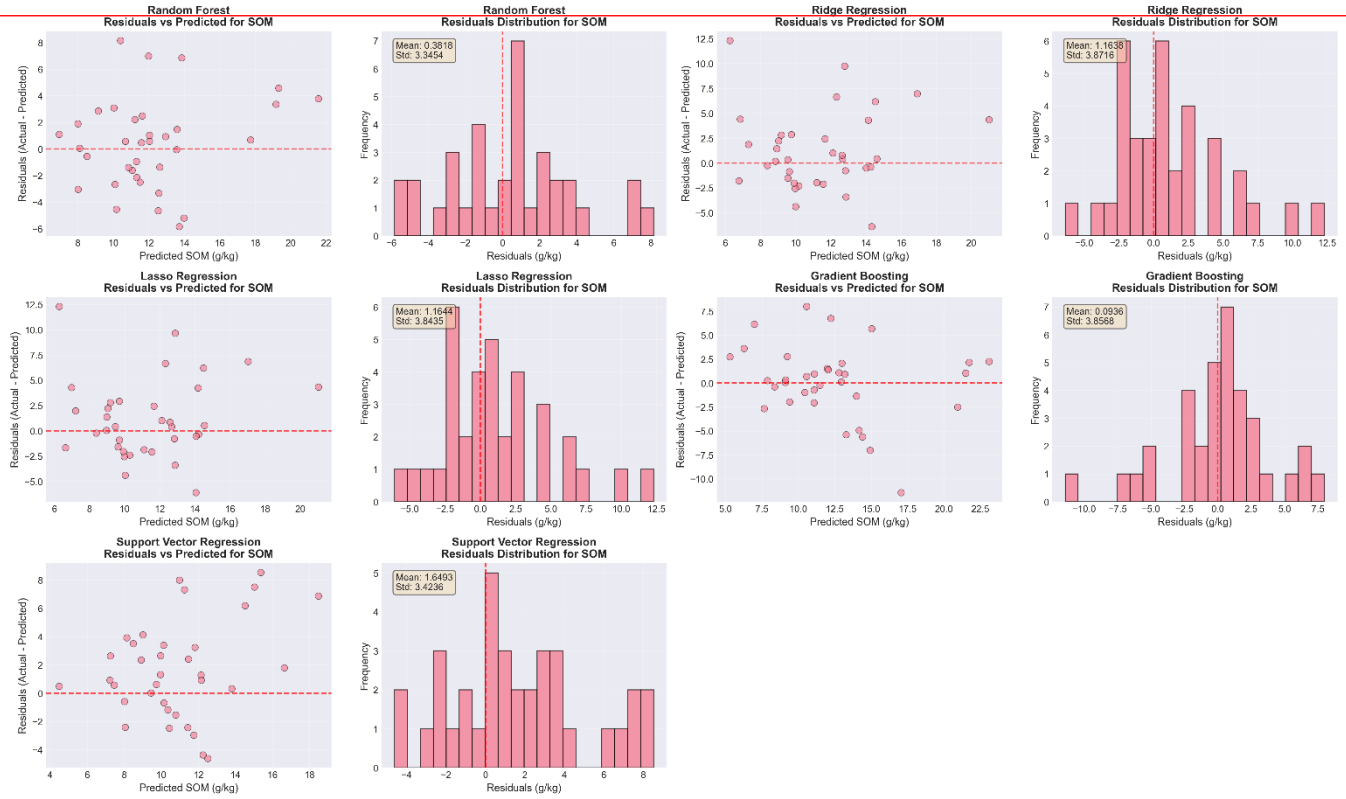

Figure 9: Residual Analysis Plots for the Five Models

3.1.3 Comparison of Spatial Pattern Consistency in the Model Predictions

To comprehensively evaluate and compare the predictive behaviors of each model from the perspective of spatial visualization, we produced comparative spatial distribution maps of the predictions from six models, namely, support vector regression, ridge regression, random forest, LASSO regression, gradient boosting, and self-organizing map models (Figure 10).

The analysis revealed the following key and robust findings: although the models differed in terms of absolute accuracy metrics for the test set (R^2 and RMSE; Table 1) and exhibited varying tendencies toward overfitting during training, the macrolevel spatial patterns of the soil organic matter (SOM) predictions were highly consistent. As shown in Figure 10, all five supervised regression models clearly exhibited a common core pattern, namely, the SOM values in the hilly and forested regions in the eastern and western parts of the study area were high, whereas those in the broad central river valleys and intensive agricultural zones were notably low. This cross-algorithm consistency, which spans linear, nonlinear, and ensemble model families, provides convincing spatial evidence that the core regional SOM distribution pattern of high values in the east and west and low values in the central region is reliable. These findings indicated that this pattern was not an artifact of any

specific model but rather an intrinsic soil landscape differentiation consistently revealed through multiple independent modeling approaches.

While the overall spatial patterns were consistent, the different models exhibited notable differences in terms of the smoothness of the predicted surfaces and local variability, reflecting their underlying algorithmic characteristics. The predictions from the random forest and gradient boosting models were the smoothest, as they revealed natural spatial gradients and effectively captured the continuous variation in soil properties across the landscape. In contrast, the predictions from the ridge and LASSO regression models indicated more notable local patchiness or striping noise, likely because of the limited ability of these linear models to capture complex nonlinear relationships and interactions, as well as their higher sensitivity to multicollinearity among high-dimensional features. The prediction results from the support vector regression model revealed intermediate smoothness between these two groups.

Moreover, the self-organizing map (SOM) model shown in Figure 10, as an unsupervised clustering approach, produced output values whose physical meaning differs from that of the regression-predicted SOM content (g/kg). The output is more indicative of spatial clusters of soil types or landscape units defined by multivariate environmental features. The patchy spatial structures generated by this model corresponded closely to the high- and low-value areas predicted by the supervised models (e.g., specific SOM clusters overlapped with high-value zones predicted by the random forest model), indirectly corroborating, from another perspective, the systematic intrinsic relationship between environmental covariates and the spatial heterogeneity in SOM.

In summary, from the perspective of spatial patterns, it was confirmed that the random forest model not only preserved the macrolevel predictive consistency observed across other models but also generated more reasonable and smoother spatial details. This finding in turn supported its selection as the optimal mapping model for subsequent in-depth analysis.

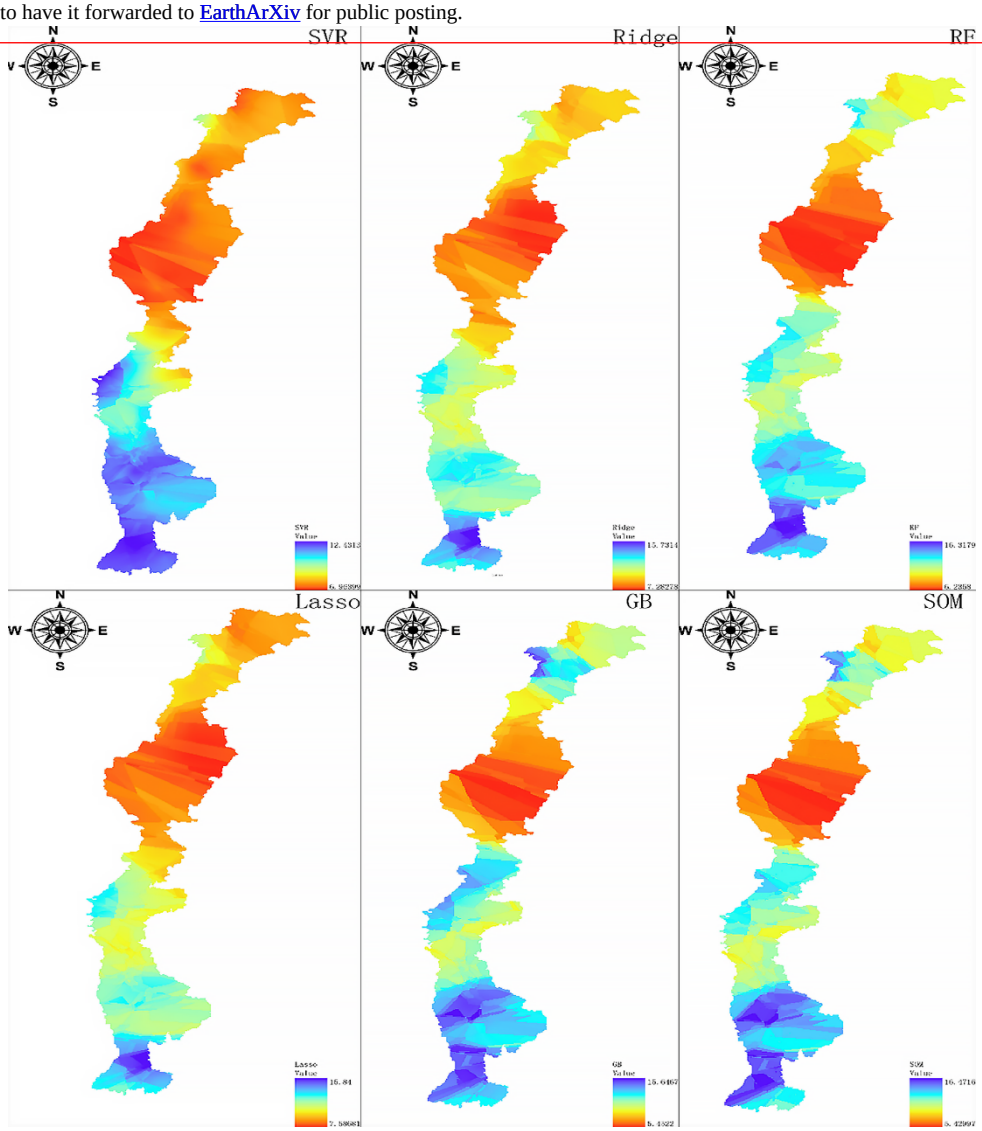

Figure 10: Comparative Spatial Distribution Maps of the Prediction Results

3.2 Feature Importance and Spatial Prediction of the Optimal Model (Random Forest)

After identifying the random forest (RF) model as the optimal prediction model, we employed it to spatially predict the soil organic matter (SOM) content in all pixels across the entire study area.

The predicted SOM concentrations ranged from 5 to 35 g/kg, indicating a clear bimodal distribution. The first major frequency peak occurred at approximately 15–20 g/kg, whereas a higher second peak was observed at 28–32 g/kg. This bimodal pattern strongly suggested the presence of two dominant and systematic SOM states or underlying land use/cover conditions in the study area.

In terms of central tendency, the mean predicted value was 21.50 g/kg, and the median was 20.46 g/kg, which are relatively close. The mean was slightly greater than the median, indicating a slight right skew (positive skewness), which was caused primarily by pixels in the high-value region (the second peak). The overall shape and statistics of this distribution provided an important quantitative context for understanding the subsequent spatial heterogeneity: when high- or low-value areas were identified spatially, their deviation from the overall level could be immediately assessed relative to this global distribution.

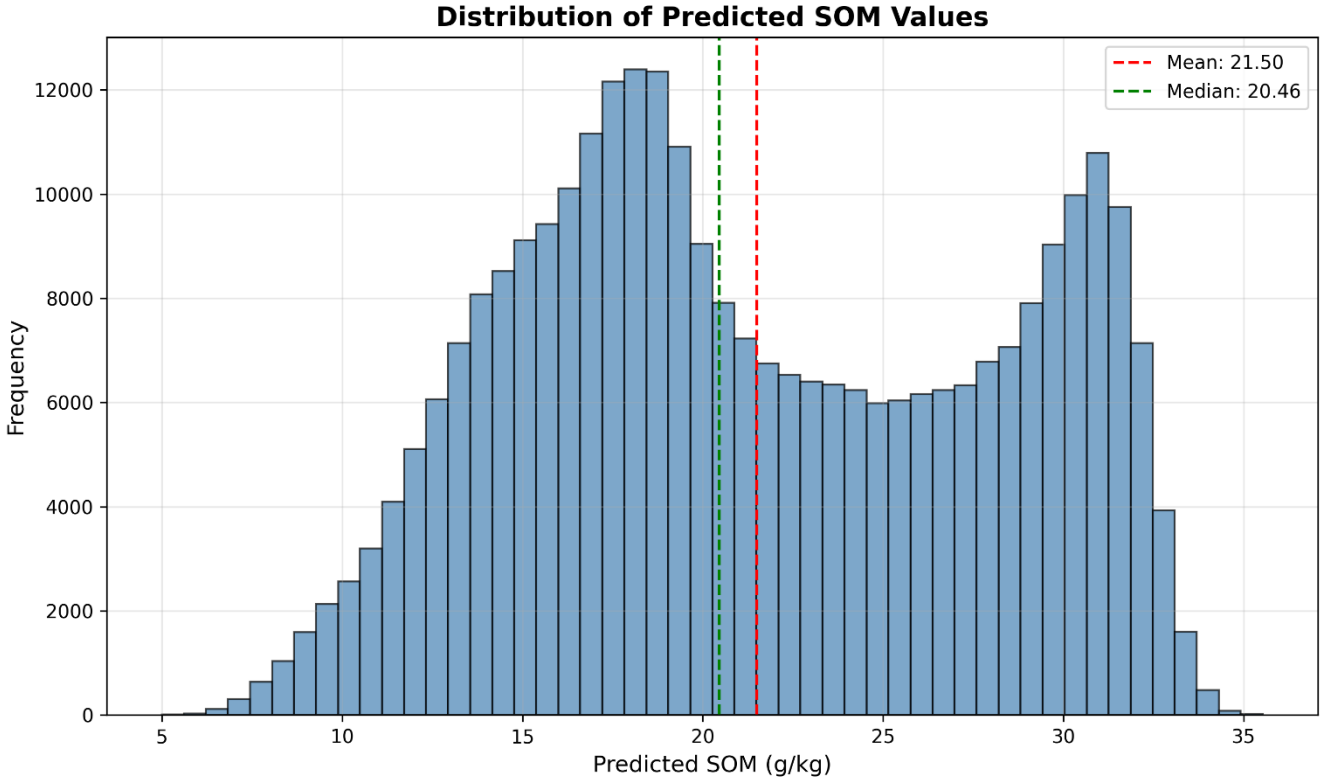

Figure 11: Frequency Distribution Histogram of Soil Organic Matter Contents Predicted by the Random Forest Model

3.2.1 Feature Importance Analysis: Identifying the Key Driving Factors

On the basis of the optimal RF model, we assessed the contributions of variables using both the Gini and permutation importance methods (Figure 12). Both approaches consistently identified available phosphorus (Avail. P) as the most important predictive variable, followed by exchangeable potassium (Ex-K), pH, and topographic factors (slope.1 and TPI). These findings highlight the critical influence of soil nutrient status on the spatial heterogeneity in SOM.

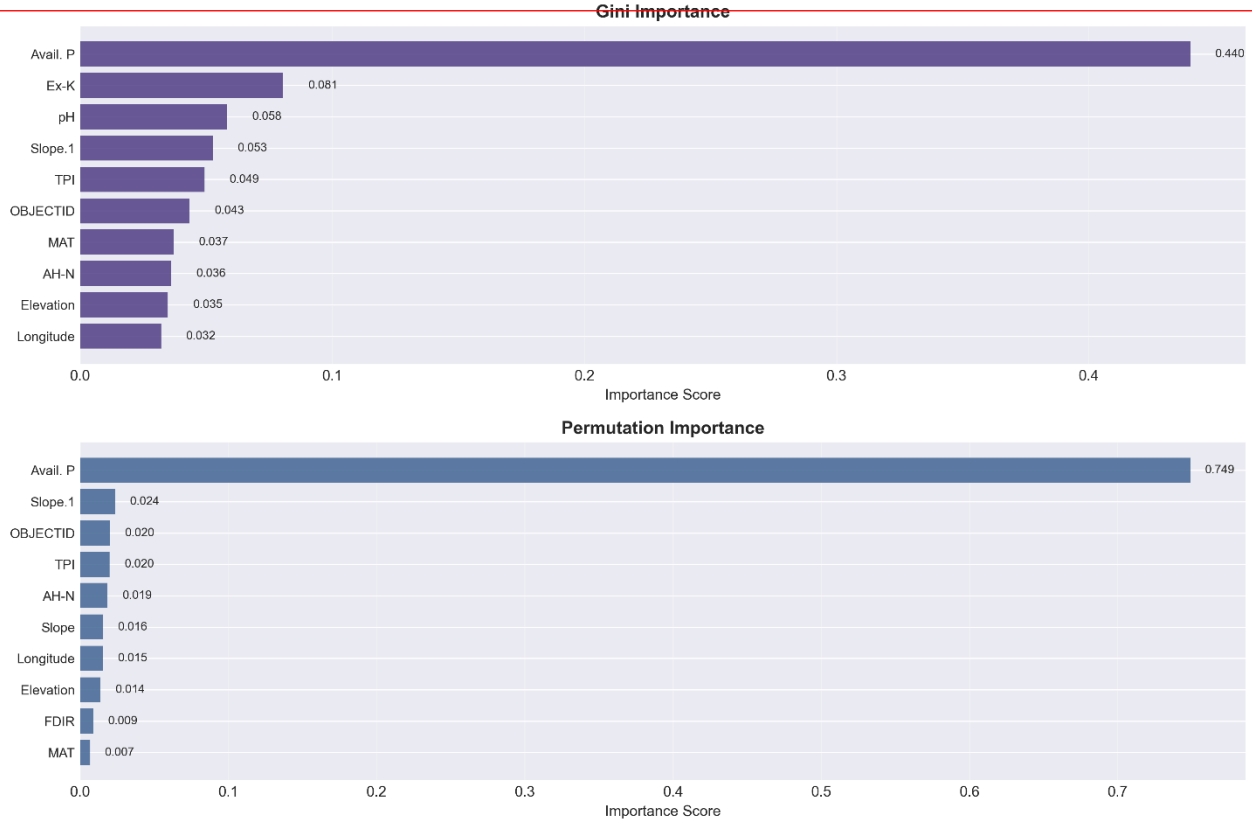

Figure 12: Feature Importance Ranking of the Random Forest Model (Gini Importance and Permutation Importance)

On the basis of the optimal random forest model, we evaluated the contributions of environmental variables using both Gini and permutation importance indices. The results from the two methods were highly consistent. Both clearly identified available phosphorus as the most important variable for predicting the spatial distribution of SOM, with an importance score far exceeding that of the other factors. This variable was followed by exchangeable potassium, pH, and topographic factors. These findings strongly indicated that the soil nutrient status, particularly phosphorus availability, was the key driving factor controlling the spatial heterogeneity in SOM across the thirteen counties in the Yellow River Basin, surpassing the traditionally recognized dominance of climatic or purely topographic factors.

3.2.2 Spatial Pattern Validation: Macroscale Robustness and Microscale Mechanism Revelation

To assess the reliability of the spatial patterns shaped by the identified driving factors, we examined the prediction results at different spatial scales (Figure 13). The results indicated that from the 1× to 4× scale, the core spatial pattern, i.e., high SOM contents in the eastern and western hilly forested areas and low contents in the central river valley agricultural regions, remained consistent. This scale invariance demonstrated that the patterns captured by the model were not random local noise but reflected stable, intrinsic soil–landscape relationships within the study area, thereby greatly enhancing the credibility and practical value of the findings.

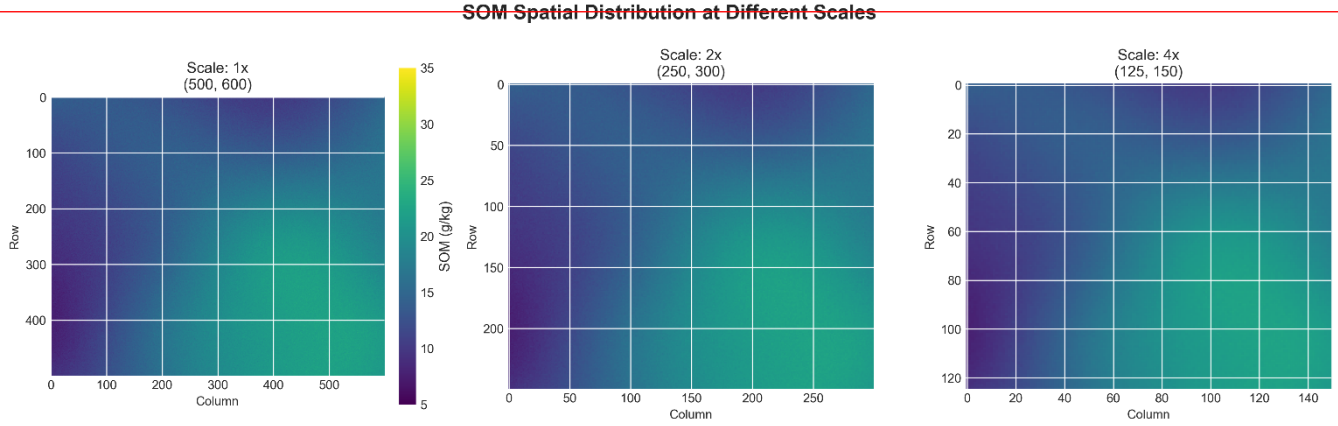

Figure 13: Comparative Spatial Distributions of SOM at Multiple Scales

Feature importance analysis revealed elevation as a key topographic factor. To elucidate its specific mechanism, we conducted a microscale analysis along typical topographic transects (Figure 14). The analysis revealed that the SOM content was significantly positively correlated with elevation along both the horizontal and vertical transects, confirming that elevation influences the accumulation of SOM by regulating hydrothermal conditions and erosion processes. However, the correlation along diagonal transects was weaker, suggesting that local anthropogenic activities (e.g., agriculture on specific slope aspects) may have interfered with or overridden the effect of this natural driving factor. These findings indicated that in practical management, when macrolevel strategies (e.g., conserving high-elevation forests) are implemented, managers should consider differentiated microscale management.

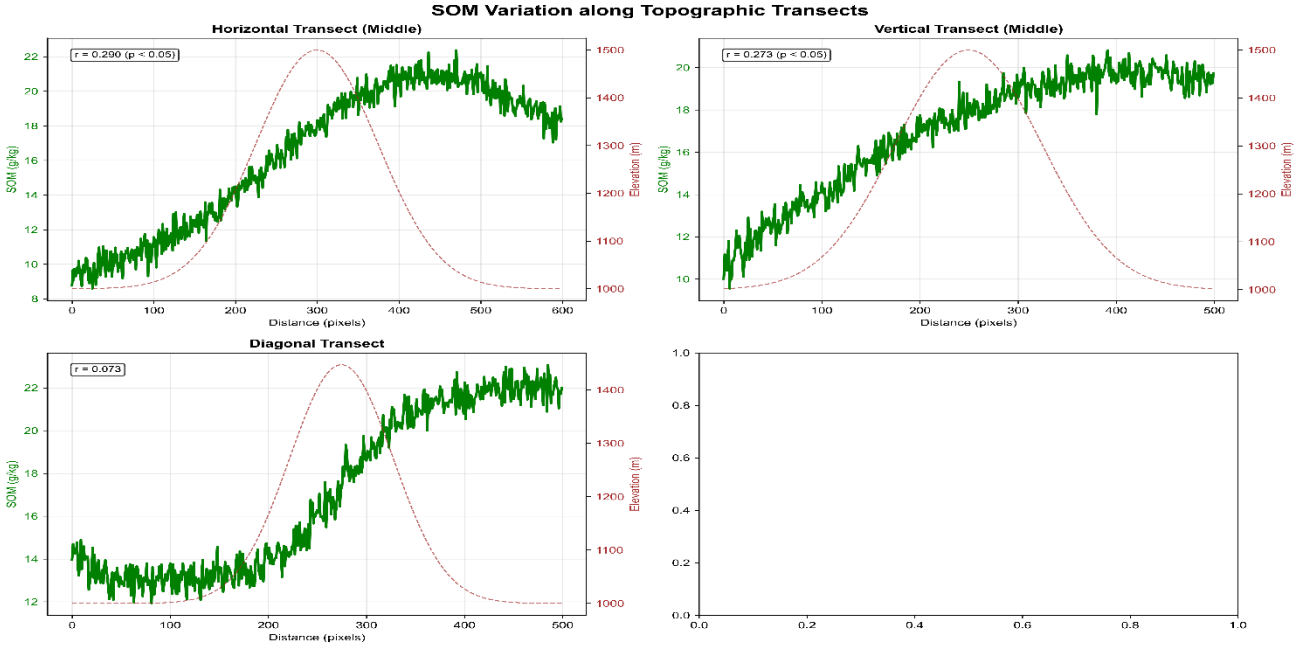

Figure 14: Analysis of the Variations in the SOM Content along Topographic Transects

3.3 County-Scale Analysis of SOM Differences Based on the Optimal Model

On the basis of the continuous spatial prediction map generated by the optimal random forest (RF) model, we analyzed in depth the spatial heterogeneity in SOM in the typical elongated counties of the Yellow River Basin. To evaluate the effectiveness of the prediction model and reveal potential underlying data structures, we also employed a self-organizing map (SOM) model for comparative analysis, with the results shown in Figure 15.

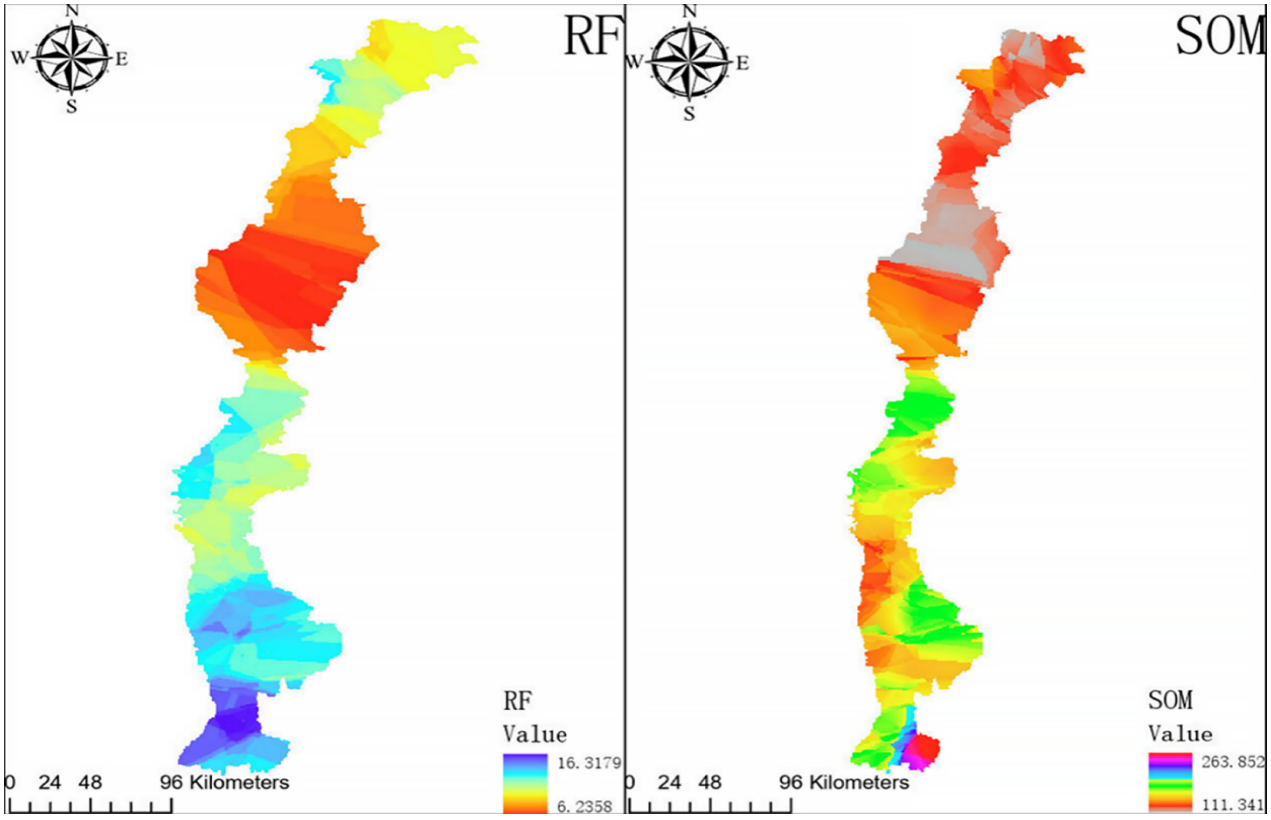

Figure 15: Comparison of County-Scale SOM Predictions Based on the Random Forest (RF) and Self-Organizing Map (SOM) Models

3.3.1 S Continuous Spatial Pattern Revealed by the RF Model

As shown in the left panel of Figure 15 (RF model), the predicted soil organic matter values (RF model values) exhibited a clear south-to-north continuous gradient within the county, with values ranging from 6.23 to 16.34 g/kg, which is consistent with typical surface soil SOM levels. The color gradient transitioned from deep blue–purple in the southern low-value areas to bright red in the northern high-value areas, clearly indicating the systematic influence of environmental drivers, such as elevation, climatic gradient, and vegetation cover, on the accumulation and decomposition of SOM. Spatial continuity demonstrated that the RF model successfully captured the gradual variation in soil properties across the natural landscape, and

the predictions can be used directly to identify priority zones for soil fertility enhancement (e.g., southern low-value areas) and key regions for ecological protection (e.g., northern high-value areas).

3.3.2 Classification Patterns of the SOM Model and Comparative Insights

The right panel of Figure 15 shows the output of the self-organizing map (SOM) model (SOM model values). This model is typically employed for clustering, dimensionality reduction, and visualization of high-dimensional data. Its output values (which range from 111.34 to 263.85 in the figure) do not correspond directly to the conventional SOM content (g/kg) but rather likely represent a spatial classification index of soil types or states defined by a combination of multiple environmental variables. Compared with the RF map, the spatial distribution (with colors ranging from pink and red–orange to gray) exhibited a patchier and more discontinuous pattern. This difference has important methodological implications.

Mechanistic Differences: The RF model provides regression analysis of a continuous target variable, whereas the SOM model is an unsupervised neural network designed to reveal intrinsic structures and clustering patterns in the data. The physical meaning and numerical scale of their outputs fundamentally differ.

Complementary Applications: The patchy structures revealed by the SOM model map may correspond to abrupt boundaries of soil types, parent materials, or microtopography, providing important complementary information to the continuous environmental gradients captured by the RF model. At the application level, the above suggests that managers should not only consider the continuous variation in the SOM content (RF model results) but also account for abrupt differences between land units or types (SOM model results) to develop more targeted, site-specific management strategies.

3.3.3 *Support for Differentiated Governance Based on Integrated Comparison*

By juxtaposing the two maps (Figure 15), this study provided dual and complementary spatial evidence to support its core application objective, i.e., to ensure differentiated county-level governance:

The RF model results provided degree guidance: The results clearly indicated a SOM gradient ranging from poor to fertile within the county from south to north, offering a direct basis for implementing quantitative management measures such as organic fertilizer allocation and conservation tillage.

The SOM results provided type boundaries: The patchy distribution of the results suggested the existence of potential management subdivisions (e.g., different soil type zones or land use history units), indicating that the policy intensity and management approaches should be adjusted across these subregions.

Therefore, the integrated analysis results shown in Figure 15 suggested that the combined interpretation of the results of the optimal RF model and the SOM model results not only provided a high-precision characterization of the quantitative spatial distribution of the SOM content but also aided in understanding the structural drivers of its spatial heterogeneity. This laid a solid foundation for translating scientific predictions into a comprehensive management base map that integrated degree grading and type partitioning, thus ensuring that the subsequent governance recommendations, such as the delineation of enhancement and core conservation zones, are supported by both quantitative standards and clearly defined spatial boundaries.

3.4 Integrated Comparison and Differential Diagnosis of County-Scale Spatial Patterns Based on the Optimal Model

To directly address the research objective of quantifying SOM differences among the thirteen county-level administrative units and to establish a spatial decision-making foundation for differentiated governance, this section presents detailed spatial distribution maps of soil organic matter across all thirteen counties on the basis of the optimal random forest model (Figure 16), accompanied by systematic statistical comparisons (Figure 17).

3.4.1 Panoramic Visualization of County-Scale SOM Spatial Patterns

As shown in Figure 16, this study, for the first time, systematically revealed the spatial heterogeneity in SOM within each administrative county via a unified professional mapping standard. This series of thematic maps clearly decomposed the macroscale basin pattern of high values in the east and west and low values in the central region and anchored it within specific county-level administrative units.

High-value counties: Central–southern counties such as Wanrong and Hejin generally exhibited high predicted SOM values, corresponding to the widespread warm-colored areas in the maps.

Low-value counties: Northwestern counties such as Xingxian, Linxian, and Liulinxian revealed largely low predicted SOM values, represented mainly by cool-colored areas.

Transition counties: The remaining counties indicated a mix of high and low values or contiguous areas of moderate SOM contents, reflecting the complex landscape shaped by the combined effect of topography and land use.

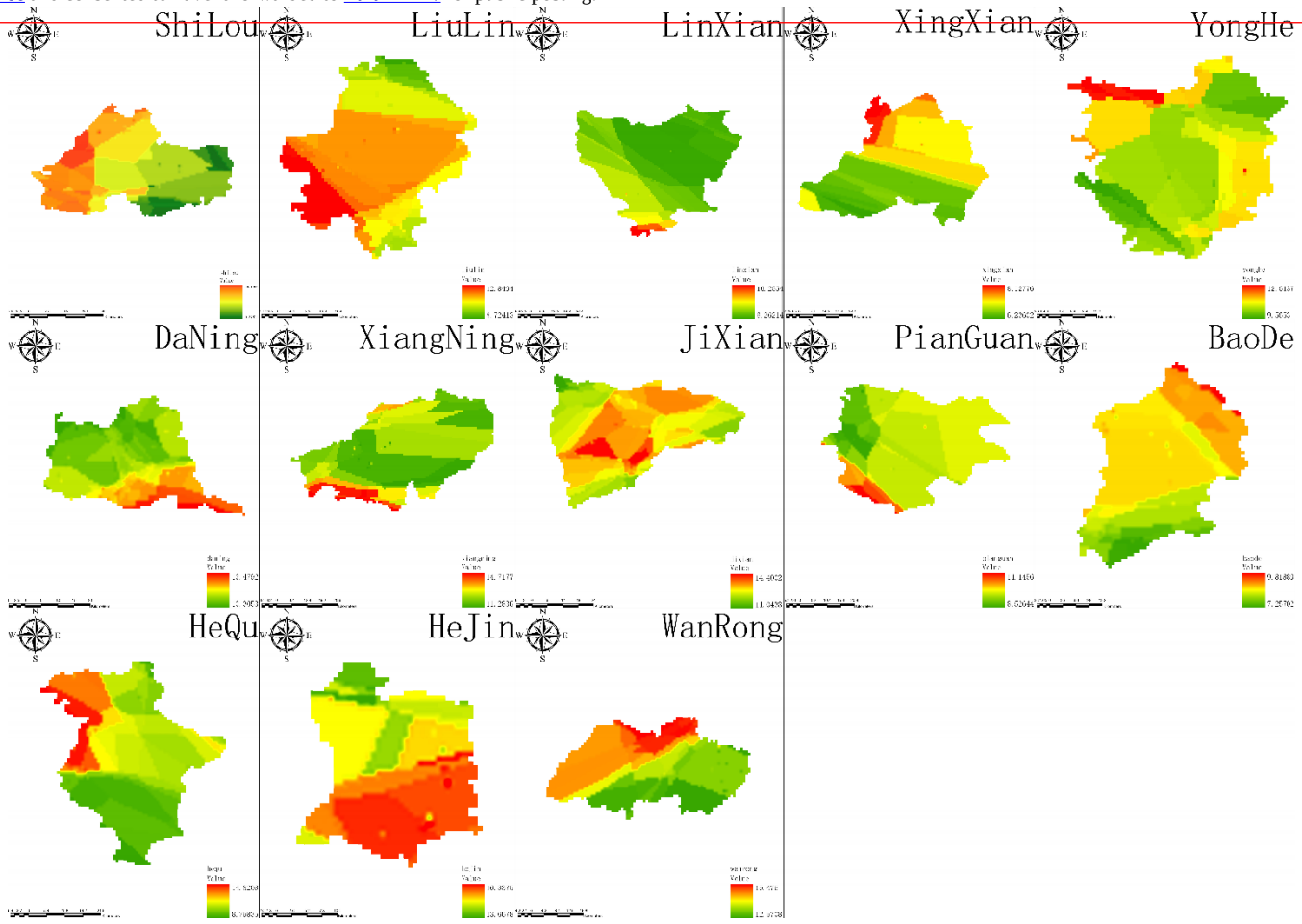

Figure 16: Detailed Spatial Distributions of Soil Organic Matter in Thirteen Counties in the Yellow River Basin Predicted by the Optimal Random Forest Model

3.4.2 Statistical Analysis of Intercounty Differences in the Mean SOM Content

To quantify the overall differences among counties, we statistically analyzed the predicted SOM values for all pixels within each county. The results of one-way ANOVA indicated that the mean SOM content differed highly significantly among the thirteen counties ($p < 0.001$). Specific statistical comparisons are shown in Figure 17.

High-value group: Hejin city and Wanrong County attained the highest mean SOM contents, at approximately 14.2 and 13.8 g/kg, respectively, and constituted the first tier.

Low-value group: Linxian, Shilou County, and Liulin County exhibited the lowest mean SOM contents, which varied between 7.0 and 7.5 g/kg, indicating the formation of a notable low-value zone.

Medium-value group: The mean SOM contents in the remaining counties, such as Jixian, Xiangning, and Daning, ranged from 8.5 to 12 g/kg, indicating the formation of the primary intermediate gradient.

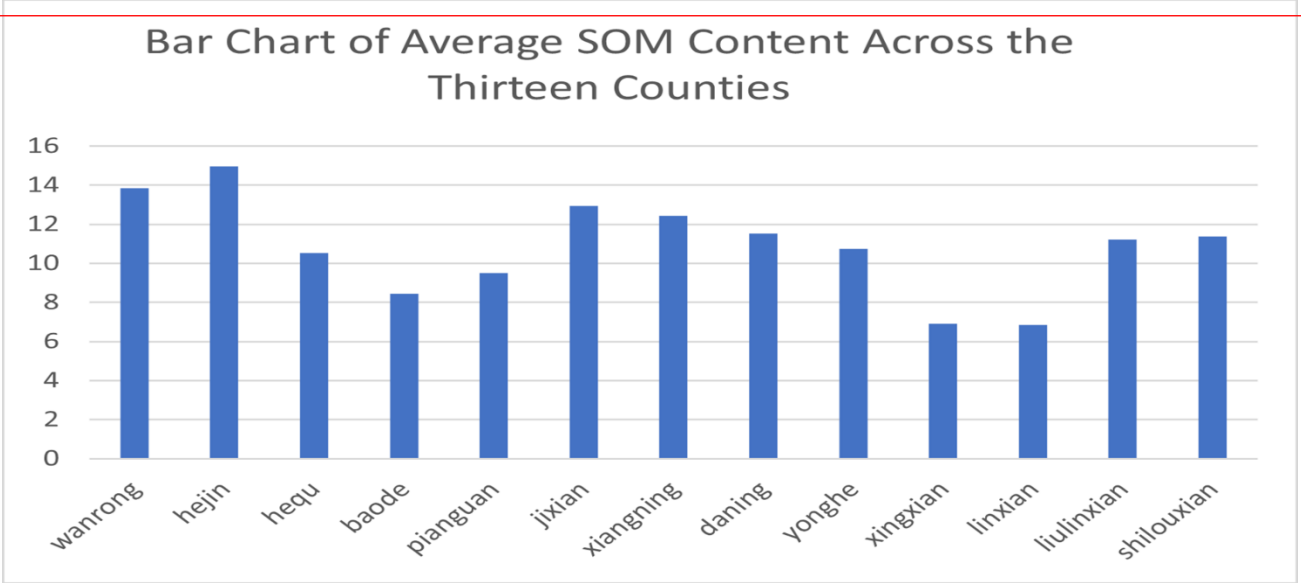

Figure 17: Statistical Comparison of the Mean Soil Organic Matter Contents across Thirteen Counties in the Yellow River Basin

3.4.3 Implications for Differentiated Governance

The spatial maps (Figure 16) and statistical tables (Figure 17) generated in this section jointly provide a dual diagnostic framework for county-level SOM management. The spatial targets for governance are shown in Figure 16, and the priority ranking for resource allocation is shown in Figure 17. Together, they provide clear guidance for precise, county-specific management strategies:

Core SOM Enhancement Zones: We clearly identified counties such as Linxian, Liulin, and Shilou as concentrated low-value areas in both the spatial maps and the statistical data. These counties should be designated urgent SOM enhancement zones, where resources for conservation tillage, straw return, and organic fertilizer subsidies should be prioritized, thereby implementing the core strategy of carbon augmentation and disturbance control.

SOM Consolidation and Optimization Zones: In high-value counties such as Hejin and Wanrong, the focus should be on consolidating advantages and optimizing the structure, protecting existing high-yield farmland, and optimizing fertilization management to maintain and enhance soil fertility. In the numerous medium-value counties, a site-specific approach should be implemented, thereby prioritizing SOM enhancement in low-value patches while strengthening protection in high-value patches.

Precise Implementation of Governance: The government of each county can use its detailed spatial map (Figure 16) to deconstruct county-level statistical targets to the township or specific watershed level, thereby formulating more actionable plans. In this way, scientific findings at the watershed scale can be effectively translated into concrete actions at the county scale.

4. Discussion

In this study, the performance of five machine learning models in predicting the spatial distribution of soil organic matter across thirteen counties in the Yellow River Basin was comprehensively evaluated. Model performance levels were systematically compared, the results of the optimal model were interpreted, and the predictions were translated into actionable insights.

4.1 Scientific Basis for Model Selection: Accuracy, Overfitting, and Context-Specific Decision Framework

The RF model was selected as the optimal choice because of its superior prediction accuracy and robust error characteristics. However, awareness of its notable tendency to overfit necessitates a pragmatic, context-dependent model selection framework that balances accuracy and stability. The results of systematic comparisons confirmed the superiority of the RF model in this landscape, with the highest test set R^2 (0.5605) and lowest RMSE (3.3671 g/kg) values among the five models (Table 1; Figure 8). These results aligned with the findings of numerous studies documenting the effectiveness of RF models in digital soil mapping, attributing this to their ability to manage nonlinear relationships, high-dimensional data, and complex interactions without requiring strict preprocessing [6,7]. Residual analysis of the model (Figure 9) also corroborated its reliability, as it revealed minimal systematic bias and homoscedastic errors.

However, a more nuanced understanding was obtained from the learning curves (Figure 4) and performance metrics (Figure 6). Although the RF model achieved high accuracy, it exhibited a substantial generalizability gap (0.305) and a large difference between the training and test R^2 values (0.826 vs. 0.560), suggesting high variance and overfitting risk. This observation conformed with the fundamental concept of bias–variance trade-off in machine learning [8]. In contrast, the ridge and LASSO models, despite providing lower predictive power, revealed minimal generalizability gaps, thus demonstrating excellent stability. This pattern presents practitioners with a critical trade-off to consider.

Therefore, our study went beyond simply identifying a best-performing model. We proposed a scenario-based selection framework: notably, for scientific mapping or compiling detailed inventories aiming for the highest accuracy in well-sampled regions, we suggest a carefully tuned and validated RF model, provided that its predictions are accompanied by explicit uncertainty quantification. For operational monitoring, rapid regional assessments, or scenarios with limited and potentially unrepresentative data, regularized linear models may offer a more robust and practical choice because of their greater stability, computational efficiency, and interpretability. This framework strengthens the methodological contribution of our work and provides guidance for future studies and applications in similarly complex terrains.

4.2. Revealing the Dominant Spatial Drivers: From Macroscopic Topography to Microscopic Nutrient Limitation

Interpretation of the results of the optimal random forest (RF) model revealed a scientifically significant finding, namely, soil available phosphorus (Avail. P) emerged as the most critical predictor of the spatial variation in SOM across the thirteen counties along the Yellow River, surpassing the importance of conventional topographic and climatic factors. This

discovery refines the driving mechanism of SOM spatial prediction from the macroscale climate–topography paradigm to a topography–nutrient synergistic framework [9, 11], offering a novel perspective for understanding soil carbon dynamics in this region.

Although the robust, multiscale spatial pattern of high values in the east and west and low values in the central region predicted by all the models confirms the overarching control of the landscape position and erosion–deposition processes, the dominance of Avail. P suggests a more nuanced biogeochemical control mechanism operating within this topographic template. In the terrestrial ecosystem of the Loess Plateau, phosphorus is often a limiting nutrient because of the calcareous soil properties in the region, which facilitate the precipitation and adsorption of phosphorus, reducing its bioavailability [10, 31]. The prominent role of Avail. P suggests that phosphorus availability may serve as a key rate-limiting or regulatory factor for SOM stabilization in this area. Phosphorus is fundamental for microbial activity, enzyme production, and the formation of organomineral complexes [10, 11, 33]. High phosphorus availability can stimulate microbial growth and enzymatic hydrolysis, thereby potentially accelerating the initial decomposition of fresh organic matter. However, high phosphorus availability may also promote the microbial transformation of organic carbon into more stable forms or enhance its association with mineral surfaces (e.g., binding with calcium or iron oxides prevalent in loess soils), thereby promoting long-term sequestration [11, 33]. Conversely, phosphorus limitation could constrain microbial processing and the formation of mineral-associated organic matter, leading to divergent patterns of SOM accumulation across the landscape. This insight shifts the perspective from focusing solely on carbon input (governed by vegetation and climate) to an integrated view that accounts for the stoichiometric balance and microbial mediation processes, highlighting the potential for carbon–phosphorus comanagement strategies.

This microscale driver operates within a robust macroscale spatial framework. The predicted spatial structure and its consistency across scales confirm a stable, landscape-driven distribution of SOM. The synergistic relationship is clear, i.e., the topography establishes the fundamental framework, whereas soil available phosphorus fine-tunes the SOM content within that framework. This refined topography–nutrient driver framework provides a more mechanistic understanding for interpreting SOM heterogeneity in the Yellow River Basin, suggesting that management practices aimed at enhancing soil carbon sequestration should account for the phosphorus status to be more effective [11, 33].

4.3 From Predictive Maps to Decision Support Tools: Enabling County-Level Differentiated Governance

In this study, we successfully transformed the continuous predictions of the RF model into a spatially explicit decision support system, thereby incorporating statistical benchmarks and comparative analyses. This approach facilitated the formulation of targeted, county-level soil management strategies, thereby bridging the gap between scientific research and policy implementation.

The ultimate value of digital soil mapping lies in providing information for ensuring sustainable land management [12]. Our study decisively moved from prediction to application. County-level statistical comparisons (Figure 17) and detailed spatial maps for each county (Figure 16) jointly provide a diagnostic dashboard for local managers.

On the basis of this dashboard, the following clear and differentiated governance strategies can be formulated:

Priority SOM Enhancement Zones: Counties with statistically low SOM contents and spatially concentrated low-value areas (e.g., Linxian, Liulin, and Shilou) should be designated high-priority intervention zones. Management should focus on carbon augmentation and disturbance control, enforcing conservation tillage, promoting deep straw incorporation, and applying targeted organic amendments. Critically, insights into the importance of phosphorus should be integrated into precise phosphorus management efforts to potentially increase the effectiveness of carbon sequestration measures.

SOM Conservation and Optimization Zones: Counties with relatively high average SOM levels (e.g., Hejin and Wanrong) should adopt strategies focused on conservation and optimization management to protect existing soil carbon stocks and optimize productivity. In counties with moderate SOM levels, management should be spatially differentiated, thereby applying intensified measures in local low-value patches, whereas high-value areas should be protected.

Precision of Policy Implementation: The complementary insights derived from the RF (continuous gradient) and SOM (clustering pattern) model results for the example counties (Figure 15) highlighted that management must account for both the degree of SOM depletion (from the RF model results) and the type of landscape or soil units (as indicated by SOM model-based clustering). This approach can facilitate precise, within-county management, moving beyond one-size-fits-all county-level policies.

5. Conclusions

In this study, five machine learning models, i.e., random forest, ridge regression, LASSO regression, gradient boosting, and support vector regression, were systematically compared to providing a complete framework for the spatial prediction and precise management of soil organic matter across thirteen counties in the Yellow River Basin, spanning model selection, mechanistic interpretation, and decision support. The core findings and contributions are as follows:

First, this study established the superior performance of the random forest (RF) model in predicting the spatial distribution of soil organic matter (SOM) across this complex watershed landscape. The RF model achieved the highest prediction accuracy for the independent test set ($R^2 = 0.560$; RMSE = 3.367 g/kg), and its prediction residuals exhibited favorable statistical properties. These findings confirmed the advantage of ensemble learning algorithms in capturing complex nonlinear relationships between environmental factors and soils [13]. More importantly, by thoroughly analyzing the learning curves and generalizability gaps of the models, we went beyond simply selecting the best-performing model and proposed a scenario-based model selection trade-off framework. This framework clearly indicates that, for scientific studies aiming for maximum accuracy, a fully validated RF model is the ideal choice, whereas for operational monitoring scenarios that prioritize stability, interpretability, and computational efficiency, linear models, such as the ridge regression model, provide a more reliable baseline tool because of their exceptional robustness [8]. This methodological contribution enhances both the practicality and scientific rigor of digital soil mapping for diverse real-world applications.

Second, in-depth interpretation of the optimal model results revealed a scientifically significant finding, i.e., available soil phosphorus was the most critical factor driving the spatial heterogeneity in SOM in this region, far surpassing the importance of traditionally recognized topographic and climatic factors. This discovery extends the mechanistic understanding of SOM spatial prediction from the macroscale climate–topography paradigm to a topography–nutrient synergistic framework [9,11]. These findings strongly suggest that, in this part of the Yellow River Basin, phosphorus availability may have a key influence on soil carbon sequestration by regulating microbial activity and organic matter turnover. This framework provides a novel theoretical perspective and empirical basis for exploring phosphorus–carbon comanagement strategies in agriculture aimed at simultaneously enhancing soil fertility and the carbon sequestration potential [10].

Finally, and most importantly, the core value of this study lies in successfully transforming model-based scientific predictions into a spatial decision-support toolkit that directly informs county-level differentiated governance. By generating high-resolution SOM spatial distribution maps (Figure 13) and quantitative intercounty statistical comparisons (Figures 16 and 17), the study provided a clear and actionable data foundation for precise, county-specific soil management. The results explicitly identified priority SOM enhancement zones (e.g., concentrated low-value areas such as Linxian and Liulin) and core SOM conservation zones (e.g., high-value areas such as Hejin and Wanrong), and differentiated strategies of carbon augmentation and disturbance control and conservation and stabilization were proposed. This framework effectively bridges the last-mile gap between digital soil mapping research and local governance practices, thus completing the full cycle from data to analysis to decision-making, and provides robust scientific support for promoting sustainable agricultural development and ecological protection in the Yellow River Basin [18].

This study exhibits several limitations. For example, it relies primarily on static environmental variables. Hence, future work should aim to integrate temporal remote sensing data to monitor SOM dynamics. In addition, the underlying microbiological and biogeochemical mechanisms driving the dominant role of available phosphorus require further field-based validation. The methodological framework and spatial datasets developed in this study can serve as benchmarks and inputs for coupling with process-based models to assess the soil carbon sequestration potential under different management practices, thereby supporting the development of more advanced intelligent decision-support systems.

Code and data availability

The soil sampling data, including soil organic matter content, that support the findings of this study are available from the corresponding author, Haibin Wang, upon reasonable request. The original data were collected by the research team from Shanxi Agricultural University. Processed and cleaned versions of these data are also being archived in a publicly accessible repository and will be available upon publication or from the corresponding author. The topographic covariates were derived from the publicly available ASTER GDEM. Climate and vegetation data were pro-cessed using Google Earth Engine.

Author contributions

Ziyang Zhang conducted the formal analysis, performed validation and visualization, and wrote the original draft of the manuscript and methodology; Ziyi Hu, Mengmeng Wu, and Liwen Liu contributed to the conceptualization and methodology of the study; Ke Hu conducted the investigation and secured the necessary resources for this study; Haibin Wang oversaw the project administration for this study; Qi Liu secured the funding acquisition for this research; Yaodong Jing developed the software tools, provided supervision throughout the research, and participated in reviewing and editing the manuscript; Mingxing Qin performed the data curation for this study. All authors have read and agreed to the pub-lished version of the manuscript." Please turn to the CRediT taxonomy for the term explanation. Authorship must be limited to those who have contributed substantially to the work reported.

Competing interests

The authors declare that they have no competing financial interests or personal relationships that could have appeared to influence the work reported in this paper.

Disclaimer

Copernicus Publications adds a standard disclaimer: "Copernicus Publications remains neutral with regard to jurisdictional claims made in the text, published maps, institutional affiliations, or any other geographical representation in this paper. While Copernicus Publications makes every effort to include appropriate place names, the final responsibility lies with the authors. Views expressed in the text are those of the authors and do not necessarily reflect the views of the publisher."
Please feel free to add disclaimer text at your choice, if applicable.

Acknowledgements

Special acknowledgment is extended to Dr. Ke Hu from Shanxi Agricultural University for his in-dispensable contributions to the field campaign, including the design of soil sampling networks across heterogeneous landscapes, coordination of multi-seasonal sample collection, and rigorous laboratory analyses of soil physicochemical properties. The constructive critiques provided by anonymous reviewers greatly enhanced the methodological robustness and theoretical coherence of this hybrid spatial prediction framework. Additionally,we express gratitude to the technical teams from both supporting institutions for their instrumental role in data validation and spatial database construction. Their collaborative efforts ensured the seamless fusion of ma-chinelearn-ing-driven trend surfaces with geostatistically optimized residual corrections, ulti-mately advanc-ing precision in environmental parameter estimation for complex terrain regions. This interdisci-plinary synergy underscores the critical importance of institutional collaboration in addressing spatially explicit ecological challenges.

Financial support

This research was financially supported by the Shanxi Provincial Geological Environment Monitoring and Ecological Restoration Center and Shanxi Dadi Holding Ecological Restoration Technology Co., Ltd.

Review statement

The review statement will be added by Copernicus Publications listing the handling editor as well as all contributing referees according to their status anonymous or identified.

References

1. Lal, R. Soil carbon sequestration impacts on global climate change and food security. Science2004, 304, 1623–1627.
2. Wiesmeier, M.; Urbanski, L.; Hobley, E.; Lang, B.; von Lützow, M.; Marin-Spiotta, E.; van Wesemael, B.; Rabot, E.; Ließ, M.; Garcia-Franco, N.; Wollschläger, U.; Vogel, H.; Kögel-Knabner, I. Soil organic carbon storage as a key function of soils—A review of drivers and indicators at various scales. Geoderma2019, 333, 149–162.
3. Sothe, C.; Gonsamo, A.; Arabian, J.; Snider, J. Large scale mapping of soil organic carbon concentration with 3D machine learning and satellite observations. Geoderma2022, 405, 115402.
4. Minasny, B.; McBratney, A.B. Digital soil mapping: A brief history and some lessons. Geoderma2016, 264, 301–311.
5. Heung, B.; Ho, H.C.; Zhang, J.; Knudby, A.; Bulmer, C.E.; Schmidt, M.G. An overview and comparison of machine-learning techniques for classification purposes in digital soil mapping. Geoderma2016, 265, 62–77.
6. Hengl, T.; Mendes de Jesus, J.; Heuvelink, G.B.M.; Ruiperez Gonzalez, M.; Kilibarda, M.; Blagotic, A.; Shangguan, W.; Wright, M.N.; Geng, X.; Bauer-Marschallinger, B.; et al. SoilGrids250m: Global gridded soil information based on machine learning. PLOS ONE2017, 12, e0169748.
7. Padarian, J.; Minasny, B.; McBratney, A.B. Machine learning and soil sciences: a review aided by machine learning tools. SOIL2020, 6, 35–52.
8. Hastie, T.; Tibshirani, R.; Friedman, J. The Elements of Statistical Learning: Data Mining, Inference, and Prediction, 2nd ed.; Springer: New York, NY, USA, 2009.
9. Jobbágy, E.G.; Jackson, R.B. The vertical distribution of soil organic carbon and its relation to climate and vegetation. Ecol. Appl.2000, 10, 423–436.
10. Cleveland, C.C.; Liptzin, D. C:N:P stoichiometry in soil: is there a “Redfield ratio” for the microbial biomass?. Biogeochem-istry2007, 85, 235–252.
11. Kirkby, C.A.; Richardson, A.E.; Wade, L.J.; Batten, G.D.; Blanchard, C.; Kirkegaard, J.A. Carbon-nutrient stoichiometry to increase soil carbon sequestration. Soil Biol. Biochem.2013, 60, 77–86.
12. Bouma, J. Soil science contributions towards Sustainable Development Goals and their implementation: linking soil functions with ecosystem services. J. Plant Nutr. Soil Sci.2014, 177, 111–120.
13. Breiman, L. Random forests. Mach. Learn.2001, 45, 5–32.
14. Szypłowska, A.; Lewandowski, A.; Yagihara, S.; Saito, H.; Furuhata, K.; Szerement, J.; Kafarski, M.; Wilczek, A.; Majcher, J.; Woszczyk, A.; et al. Dielectric models for moisture determination of soils with variable organic matter content. Geoderma2021, 401, 115288.

15. Dairain, A.; Maire, O.; Meynard, G.; Orvain, F. Does parasitism influence sediment stability? Evaluation of trait-mediated effects of the trematode Bucephalus minimus on the key role of cockles Cerastoderma edule in sediment erosion dynamics. Sci. Total Environ.2020, 733, 139307, doi:10.1016/j.scitotenv.2020.139307
16. Munira, S.; Farenhorst, A.; Akinremi, W. Phosphate and glyphosate sorption in soils following long-term phosphate applica-tions. Geoderma2018, 313, 146–153, doi:10.1016/j.geoderma.2017.10.030.
17. Heil, J.; Marschner, B.; Stumpe, B. Digital photography as a tool for microscale mapping of soil organic carbon and iron oxides. CATENA2020, 193, 104610, doi:10.1016/j.catena.2020.104610.
18. Ives, A.R.; Zhu, L.; Wang, F.; Zhu, J.; Morrow, C.J.; Radeloff, V.C. Statistical inference for trends in spatiotemporal data. Remote Sens. Environ.2021, 266, 112678, doi:10.1016/j.rse.2021.112678.
19. Wang, S.; Zhuang, Q.; Jia, S.; Jin, X.; Wang, Q. Spatial variations of soil organic carbon stocks in a coastal hilly area of China. Geoderma2018, 314, 8–19, doi:10.1016/j.geoderma.2017.10.052.
20. Hengl, T.; Nussbaum, M.; Wright, M.N.; Heuvelink, G.B.M.; Gräler, B. Random forest as a generic framework for predictive modeling of spatial and spatio-temporal variables. PeerJ2018, 6, e5518, doi:10.7717/peerj.5518.
21. Grimm, R.; Behrens, T.; Märker, M.; Elsenbeer, H. Soil organic carbon concentrations and stocks on Barro Colorado Island — Digital soil mapping using Random Forests analysis. Geoderma2008, 146, 102–113, doi:10.1016/j.geoderma.2008.05.008.
22. Li, J.; Lou, J.; Lv, J. The effect of sulfate on nitrite-denitrifying anaerobic methane oxidation (nitrite-DAMO) process. Sci. Total Environ.2020, 731, 139160, doi:10.1016/j.scitotenv.2020.139160.
23. Xia, J.; Ren, R.; Chen, Y.; Sun, J.; Zhao, X.; Zhang, S. Multifractal characteristics of soil particle distribution under different vegetation types in the Yellow River Delta chenier of China. Geoderma2020, 368, 114311, doi:10.1016/j.geoderma.2020.114311.
24. Parvizi, Y.; Fatehi, S. Geospatial digital mapping of soil organic carbon using machine learning and geostatistical methods in different land uses. Sci. Rep.2025, 15, 4449, doi:10.1038/s41598-025-88062-9.
25. Adeniyi, O.D.; Brenning, A.; Maerker, M. Spatial prediction of soil organic carbon: Combining machine learning with residual kriging in an agricultural lowland area (Lombardy region, Italy). Geoderma2024, 448, 116953, doi:10.1016/j.geoderma.2024.116953.
26. Keskin, H.; Grunwald, S.; Harris, W.G. Digital mapping of soil carbon fractions with machine learning. Geoderma2019, 339, 40–58, doi:10.1016/j.geoderma.2018.12.037.
27. Emadi, M.; Taghizadeh-Mehrjardi, R.; Cherati, A.; Danesh, M.; Mosavi, A.; Scholten, T. Predicting and mapping of soil organic carbon using machine learning algorithms in northern Iran. Remote Sens.2020, 12, 2234, doi:10.3390/rs12142234.
28. Lamichhane, S.; Kumar, L.; Wilson, B. Digital soil mapping algorithms and covariates for soil organic carbon mapping and their implications: A review. Geoderma2019, 352, 395–413.
29. Emami, M.; Khormali, F.; Pahlavan-Rad, M.R.; Ebrahimi, S. Predicting the spatial distribution of organic carbon in soil by combining machine learning algorithms and spline depth function in a part of Golestan Province, Iran. Soil Till. Res.2025, 251, 106530.
30. Lira Junior, M.A.; Fracetto, F.J.C.; Ferreira, J.D.S.; Silva, M.B.; Fracetto, G.G.M. Legume-based silvopastoral systems drive C and N soil stocks in a subhumid tropical environment. CATENA2020, 189, 104508, doi:10.1016/j.catena.2020.104508.

31. Tian, W.; Li, Z.; Sui, D.; Tao, Y.; Cui, Z.; Liu, B. Optimal design of a multi-dimensional validated synergistic extraction process for the treatment of atmosphere-vacuum distillation wastewater. Sci. Total Environ.2022, 817, 152986, doi:10.1016/j.scitotenv.2022.152986.
32. Eldridge, D.J.; Mallen-Cooper, M.; Ding, J. Biocrust functional traits reinforce runon-runoff patchiness in drylands. Geoderma2021, 400, 115152, doi:10.1016/j.geoderma.2021.115152.
33. Chinilin, A.; Savin, I.Y. Combining machine learning and environmental covariates for mapping of organic carbon in soils of Russia. Egypt. J. Remote Sens. Space Sci.2023, 26, 666–675, doi:10.1016/j.ejrs.2023.07.007.
34. Bania, J.K.; Nath, A.J.; Sandhya, G.; Nandy, S.; Paramesh, V.; Das, A.K. Predictive mapping of deep soil organic carbon stocks across land use systems in Southern Assam, India. Sci. Rep.2025, 15, 34253, doi:10.1038/s41598-025-16355-0.
35. Wang, C.; Li, S.-Y.; He, X.-J.; Chen, Q.; Zhang, H.; Liu, X.-Y. Improved prediction of water retention characteristic based on soil gradation and clay fraction. Geoderma2021, 404, 115293, doi:10.1016/j.geoderma.2021.115293.
36. Bullock, E.L.; Healey, S.P.; Yang, Z.; Houborg, R.; Gorelick, N.; Tang, X.; Andrianirina, C. Timeliness in forest change moni-toring: A new assessment framework demonstrated using Sentinel-1 and a continuous change detection algorithm. Remote Sens. Environ.2022, 276, 113043, doi:10.1016/j.rse.2022.113043.
37. Zhang, T.; Li, Y.; Wang, M. Prediction of soil organic carbon and total nitrogen affected by mine using Vis-NIR spectroscopy coupled with machine learning algorithms in calcareous soils. Sci. Rep.2024, 14, 28014, doi:10.1038/s41598-024-73761-6.
38. Wadoux, A.M.J.-C.; Minasny, B.; McBratney, A.B. Machine learning for digital soil mapping: Applications, challenges and suggested solutions. Earth-Sci. Rev.2020, 210, 103359, doi:10.1016/j.earscirev.2020.103359.
39. Viscarra Rossel, R.A.; Brus, D.J.; Lobsey, C.; Shi, Z.; McLachlan, G. Baseline estimates of soil organic carbon by proximal sensing: Comparing design-based, model-assisted and model-based inference. Geoderma2016, 265, 152-163, doi:10.1016/j.geoderma.2015.11.016.
40. Zhou, T.; Geng, Y.; Chen, J.; Pan, J.; Haase, D.; Lausch, A. High-resolution digital mapping of soil organic carbon and soil total nitrogen using DEM derivatives, Sentinel-1 and Sentinel-2 data based on machine learning algorithms. Sci. Total Environ. 2020, 729, 138244. https://doi.org/10.1016/j.scitotenv.2020.138244..